The structure of a statistically steady turbulent boundary layer near a free-slip surface

G. Campagne,[a] J.-B. Cazalbou,[b] L. Joly, and P. Chassaing[c]
Université de Toulouse, ISAE, BP 54032, 31055 Toulouse Cedex 4, France

(Received 27 January 2009; accepted 14 May 2009; published online 23 June 2009)

The interaction between a free-slip surface with unsheared but sustained turbulence is investigated in a series of direct numerical simulations. By changing (i) the distance between the (plane) source of turbulence and the surface, and (ii) the value of the viscosity, a set of five different data sets has been obtained in which the value of the Reynolds-number varies by a factor of 4. The observed structure of the interaction layer is in agreement with current knowledge, being made of three embedded sublayers: a blockage layer, a slip layer, and a Kolmogorov layer. Practical measures of the different thicknesses are proposed that lead to a new Reynolds-number scaling based on easy-to-evaluate surface quantities. This scaling is consistent with previous proposals but makes easier the comparison between free-surface flows when they differ by the characteristics of the distant turbulent field. Its use will be straightforward in a turbulence-modeling framework. © *2009 American Institute of Physics*. [DOI: 10.1063/1.3156014]

I. INTRODUCTION

As is well known, the properties of the fluctuating field in a bounded turbulent flow essentially differ from those observed in freely evolving flows. When the boundary is a solid wall, it interacts with the flow in two ways. First, the *impermeability condition* cancels the normal component of the velocity faster than its tangential components. Second, the *no-slip condition* cancels all velocity components. The first effect is referred to as a "blocking effect," it entails anisotropy in the flow field through interactions between pressure and velocity. The second effect produces mean as well as fluctuating shear that triggers off viscous effects in the vicinity of the surface.

In this paper we shall focus on the blocking effect by considering the case in which the boundary is a *rigid, free-slip surface*, satisfying the (kinematic) impermeability and (dynamic) free-slip conditions,

$$\mathbf{u}\cdot\mathbf{n}=\mathbf{0} \quad \text{and} \quad \mathbf{t}\times\mathbf{n}=\mathbf{0}, \tag{1}$$

where $\mathbf{u}$, $\mathbf{n}$, and $\mathbf{t}$ are the velocity, surface-normal, and surface-viscous-force vectors, respectively. In practice, these boundary conditions correspond to the interface between two immiscible fluids: (i) in the limit of a zero Froude number (flat interface), and (ii) when the viscosity of the upper fluid is vanishingly small (zero shear stress). From a more fundamental point of view, it can be viewed as a first step in the study of wall-bounded turbulence. Several flow configurations that involve such a boundary can be found in literature: The free-surface channel flow has been extensively studied both experimentally[1,2] and computationally.[3–5] The interaction between a time-evolving wake and a free surface has been computationally studied by Shen *et al.*[6] (see also Refs. 7 and 8). Oscillating-grid experiments by Brumley and Jirka[9] brought information on unsheared, sustained turbulence interacting with a free surface, while direct numerical simulations (DNSs) by Perot and Moin,[10] and Walker *et al.*[11] involved decaying, initially-isotropic turbulence in the same situation. All these flow configurations differ by the nature of the distant turbulence, whether it is (i) decaying or statistically steady; (ii) subject to residual or strictly zero-mean shear; (iii) significantly or marginally anisotropic, and whether the anisotropy favors the normal or tangential velocity component. Despite these differences, most authors agree on the point that the inhomogeneous layer involves an outer "blockage" layer (also called source layer[12,13]) and an inner "slip" layer (also called viscous layer[13] or surface layer[6,7]). The presence of the blockage layer is a consequence of the impermeability condition. It can be defined as the region adjacent to the surface where the variance of the normal velocity fluctuation goes from its far-field value down to zero. The slip layer appears as a consequence of the free-slip condition, a by-product of which being that the tangential vorticity components should vanish at the surface. It can be defined as the region across which the tangential vorticity fluctuation decreases down to zero at the surface. The existence of a third *Kolmogorov* layer, located in the immediate vicinity of the surface, was reported by Brumley and Jirka[14] and Calmet and Magnaudet.[13] According to these authors, the rms value of the normal component of the fluctuation follows its (linear) asymptotic near-surface behavior in this finite thickness layer.

In Ref. 15, we have approached this problem by computing a numerical analog of the oscillating-grid experiment. A DNS was performed in which, turbulence was generated by random forcing in a finite-height region, parallel to the free-slip surface. Mean shear is not involved in the turbulence-production process, and since the forcing is sta-

[a]Present address: Civil and Computational Engineering Centre, School of Engineering, Swansea University, UK.
[b]Electronic mail: cazalbou@isae.fr.
[c]Also at INPT-ENSEEIHT-Institut de Mécanique des Fluides de Toulouse UMR 5502 CNRS.

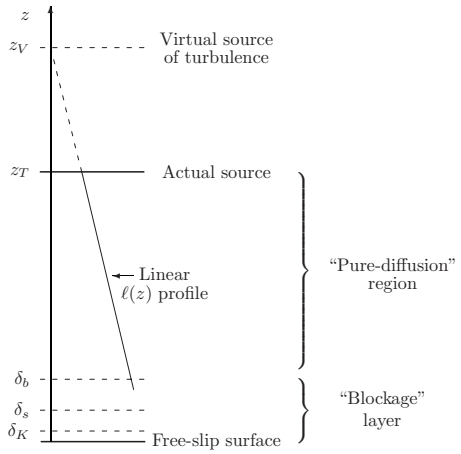

FIG. 1. Theoretical sketch of the interaction between a plane source of turbulence and a free-slip surface. The source and the surface are contained in parallel (x,y) planes.

tistically steady, the resulting flow also possesses this property. In this paper, we report the results of a comprehensive study of this flow configuration: Five different calculations have been performed in which the Reynolds number of the simulation has been varied by using different values for the viscosity and distance between the turbulence-production region and the free-slip surface. The primary objectives are to precisely define and measure the thicknesses of the different layers and provide quantitative Reynolds-number scalings that could ease the comparison with other existing data.

II. THEORETICAL CONSIDERATIONS

From a theoretical point of view, we are interested in the turbulent flow that takes place between a plane source of nearly isotropic turbulence and a free-slip surface. The source generates a statistically steady and zero-mean fluctuating velocity field in the surrounding fluid. We adopt the notation conventions given in Fig. 1. Accordingly, the source and the surface are contained in parallel (x,y) planes, the z-axis points toward the source with its origin located on the surface, the distance between the surface and the source is denoted as z_T.

Assuming that, at any location, the turbulent statistical state can be fully determined by a set of two characteristic scales (a velocity scale $\mathcal{U}$ and a length scale ℓ), the problem is fully defined by the values of the Reynolds number $\mathcal{U}_T\ell_T/\nu$ at the source (or any other convenient location) and nondimensional distance z_T/ℓ_T. If the ratio z_T/ℓ_T is large, turbulence self-diffusing from the source will not be influenced by the presence of the surface over a significant region of the flow. In this "self-diffusion" region, theory[16] and experiment[17,18] indicate that the velocity scale decreases with the distance from the source, while the length scale increases. Interestingly, most authors agree on a hyperbolic $(z_V-z)^{-1}$ behavior for the velocity scale and a linear (z_V-z) behavior for the length scale (z_V denotes a virtual origin located beyond the actual turbulent source, see Fig. 1) so that the flow should approach a constant-Reynolds-number, self-similar state in this region. This self-similar state is believed to be slightly anisotropic: according to most oscillating-grid experiments, the value of the anisotropy parameter $I=w'/u'$ (where w' and u' are the rms fluctuations along z and x, respectively) being in the range 1.1–1.3.

Denoting the thickness of the blockage layer as δ_b, one can assume that the self-diffusion regime persists down to $z=\delta_b$. A direct consequence of this assumption is that the location of the virtual origin should be uniquely defined by the values of ℓ_b (the characteristic length scale at the edge of the blockage layer) and δ_b since $z_V=\delta_b+\ell_b/\gamma$ (γ is the value of the length-scale slope in the self-diffusion regime). It follows from this simple model that the flow in the blockage layer should be independent of the actual location of the source between $z=\delta_b$ and $z=z_V$, provided that its *action parameter*[19] $K=\mathcal{U}_T\ell_T$ is taken equal to the product $\mathcal{U}_b\ell_b$. The dependency of the flow on the nondimensional distance z_T/ℓ_T is therefore removed, and any global characteristic should only depend on the value of the Reynolds number. In particular, the nondimensional thicknesses of the blockage, slip, and Kolmogorov layers may take the respective forms

$$\frac{\delta_b}{\ell_b}=f_b(\mathrm{Re}_b),\quad \frac{\delta_s}{\ell_b}=f_s(\mathrm{Re}_b),\quad \text{and}\quad \frac{\delta_K}{\ell_b}=f_K(\mathrm{Re}_b),\qquad (2)$$

where $\mathrm{Re}_b=\mathcal{U}_b\ell_b/\nu$ denotes the value of the turbulent Reynolds number at the edge of the blockage layer (and therefore in the whole of the self-diffusion region).

Similar (single-parameter) scalings can be shown to apply in the other flow configurations mentioned in Sec. I. In the case of an open channel, the flow is fully determined by the value of the friction Reynolds number, and the height of the channel is the most obvious choice to scale the different thicknesses. However, Calmet and Magnaudet[13] reported that ℓ_b can be unambiguously obtained from their large-eddy simulation (LES) data. Assuming that $\delta_b=\ell_b$, they can then evaluate $\mathcal{U}_b$ and Re_b. Accordingly, they propose scalings in the form

$$\frac{\delta_b}{\ell_b}\propto 1,\quad \frac{\delta_s}{\ell_b}\propto \mathrm{Re}_b^{-1/2},\quad \text{and}\quad \frac{\delta_K}{\ell_b}\propto \mathrm{Re}_b^{-3/4}.\qquad (3)$$

These scalings were originally introduced by Hunt and Graham[12] in their theoretical study of the interaction between decaying turbulence and a solid boundary. In this flow, a solid wall is suddenly inserted in an initially isotropic, turbulent field. At the early stages, the structure of the inhomogeneous layer depends on the time elapsed since wall insertion and a characteristic Reynolds number. At later stage, however, the evolution is believed to become self-similar and the time dependency removed, leading to scalings (3) in which the characteristic length and velocity scales ℓ_b and $\mathcal{U}_b$ can easily be assimilated to the far-field values of the rms velocity fluctuation and integral scale. In their study of time-evolving wakes near a free surface, Shen *et al.*[7] also observed that the evolution of the flow becomes self-similar at large times. The structure of the inhomogeneous layer can then be scaled by a single parameter. Shen *et al.* introduced a turbulent Reynolds number defined as the ratio of the eddy viscosity to the molecular viscosity at the outer edge of the

sheared region (outside the blockage layer). Accordingly, the proposed scalings can be simplified to

$$\frac{\delta_b}{\Delta} \propto \mathrm{Re}_t^{-1/2} \quad \text{and} \quad \frac{\delta_s}{\Delta} \propto \mathrm{Re}_t^{-1}, \tag{4}$$

where Re_t is the Reynolds number defined above and Δ is the thickness of the shear layer.

III. COMPUTATIONAL APPROACH

From a computational point of view, the ideal situation considered in Sec. II can only be approximated. The governing equations are solved on a rectangular domain, the vertical dimension of which is L_z. Impermeability and free-slip conditions (1) are imposed on the $z=0$ and $z=L_z$ boundaries under the form

$$w = 0 \quad \text{and} \quad \partial u/\partial z = \partial v/\partial z = 0.$$

The flow is assumed to be periodic in the horizontal directions, with periods L_x and L_y corresponding to the dimensions of the domain in these directions. The turbulence generating mechanism is implemented within a nonzero-height region located in the middle of the fluid layer between the top and bottom boundaries. In all the simulations, the height of this region is one third of the vertical extent of the whole layer $(L_z/3 < z < 2L_z/3)$.

Requiring, as in the theoretical model, that the distance between the turbulence source and the surface should be large compared to the turbulent scale would be very costly from a computational point of view, and has not been retained here. As a consequence, the turbulent Reynolds number is not constant above the blockage layer. The advantage is that the Reynolds-number range covered in the simulation can indeed be extended by changing the value of viscosity, but also by varying L_z; the drawback being that the surface boundary layer is not connected to a self-similar region where reference quantities such as $\mathcal{U}_b$ and ℓ_b could be unambiguously defined.

The governing equations are the continuity and Navier–Stokes equations, written for an incompressible fluid under the form

$$\nabla \cdot \mathbf{u} = 0, \tag{5}$$

$$\partial_t \mathbf{u} = \mathbf{u} \times (\nabla \times \mathbf{u}) - \nabla\left(\frac{P}{\rho} + \frac{\mathbf{u}^2}{2}\right) + \nu \nabla^2 \mathbf{u}, \tag{6}$$

where P is the pressure, and ρ and ν are the fluid density and viscosity, respectively. Time discretization of the momentum equations is based on a third-order Runge–Kutta scheme for the convective terms, and a second-order Crank–Nicholson scheme for the viscous terms. A predictor-corrector method similar to that proposed by Lamballais[20] is used at each of the three substeps of the Runge–Kutta scheme: At the predictor stage, a provisional velocity field is obtained as the solution of the momentum equation in which the pressure lags behind the velocity by one substep; at the corrector stage, a pressure-correction field is obtained from the solution of a Poisson equation. The pressure correction is then used to update the pressure field, and correct the velocity field so as to satisfy the continuity equation. The resulting scheme is second-order accurate in time. The time-discretized equations are then solved using a pseudospectral method: The linear terms are evaluated in the spectral space while the nonlinear terms are evaluated in the physical space.[21] Conventional Fourier's decompositions are used in the horizontal directions; however due to the nature of the boundary conditions at the top and bottom surfaces, the decomposition in the vertical direction makes use of simple sine or cosine series depending on the even or odd character of each variable at the surface. Orszag's 2/3 rule[22] is used for antialiasing.

Turbulence is generated in the flow by way of a random, zero-mean, three-dimensional, and isotropic force field which is added to the right-hand side of Eq. (6). Following Alvelius,[23] the random force is implemented in the spectral space, and concentrated at low wave numbers according to the power spectrum

$$E_f(\kappa) = \mathcal{P} \exp[-(\kappa - \kappa_f)^2/c].$$

The forcing wave number κ_f is taken equal to 4 and the width of the forcing spectrum around κ_f is given by the concentration parameter c. With the value $c=0.05$ used here, more than 99% of the energy input is concentrated in the range $\kappa=3.5$ to 4.5, and its amount is monitored by the value of $\mathcal{P}$ (0.025 divided by the time step, here). In order to spatially confine the forcing, the Alvelius force field is multiplied by the following function of z:

$$\mathrm{H}(z - L_z/3)\mathrm{H}(2L_z/3 - z)\cos\frac{3\pi}{2L_z}(2z - L_z),$$

where H is the Heaviside function. As a consequence of the spatial confinement of the random-force field, the turbulent velocity field slightly departs from isotropy in the forcing region. The value of the isotropy parameter settles in the range 0.8–0.9 there.

The statistics are gathered after a transient period needed for the dissipation rate to adapt to the random-force power input. The process benefits from several properties of the solution: (i) statistical homogeneity in planes parallel to the surfaces; (ii) symmetry with respect to the midplane; (iii) rotational symmetry about the z axis; (iv) statistical steadiness. At a given time, statistical quantities are calculated by first averaging over planes parallel to the free surfaces. Symmetry with respect to the midplane is then used to average the data between points located at an equal distance from each of the free surfaces. Finally, rotational symmetry is used to average the correlations involving the horizontal components of the fluctuation. The results of this process are further averaged in time with samples spaced by one half of the large-eddy turnover time τ (taken as the ratio of the volume-averaged turbulent kinetic energy to dissipation rate). Hence, for a calculation using $N_x \times N_y \times N_z$ points during a time interval equal to $N_t \times \tau$, the z-dependent statistics rely on $2N_x \times N_y \times N_t$ samples for correlations involving w, and twice that number for those involving at least one of the tangential velocity components.

TABLE I. Definition of the different simulations. In all of them, the grid size is the same in the three directions so that N_z follows from the choice of L_z. $\mathcal{U}_0=k_0^{1/2}$ and $\ell_0=k_0^{3/2}/\epsilon_0$ denote the characteristic velocity and length characteristic scales at the surface. The value of the viscosity results from the use of a $\kappa_{\max}\eta$ criterion.

Re_0	76	85	151	220	302
z_f^*	1.20	0.93	1.30	1.01	0.74
$\mathcal{U}_0/\ell_0$	0.100/1.52	0.129/1.31	0.0735/1.62	0.0956/1.82	0.144/1.66
$L_x\times L_y\times L_z$	$2\pi\times 2\pi\times 7\pi/4$	$2\pi\times 2\pi\times 7\pi/6$	$2\pi\times 2\pi\times 2\pi$	$2\pi\times 2\pi\times 7\pi/4$	$2\pi\times 2\pi\times 7\pi/6$
$N_x\times N_y\times N_z$	$192\times 192\times 168$	$192\times 192\times 112$	$384\times 384\times 384$	$384\times 384\times 336$	$384\times 384\times 224$
N_t	498	498	1206	1768	1870
ν	2×10^{-3}	2×10^{-3}	7.9×10^{-4}	7.9×10^{-4}	7.9×10^{-4}

Five different simulations have been run. In all cases, the horizontal dimensions of the domain are set to 2π and the values of the vertical dimension and viscosity fully define the problem. Both values have been varied with the requirements that the grid size remains the same in the three directions and satisfies a given resolution criterion. The traditional $\kappa_{\max}\eta$ criterion has been used; $\kappa_{\max}$ is the highest wave number resolved and η is the Kolmogorov length scale based on the volume-averaged dissipation rate. Accordingly, the value of the viscosity is adjusted so that $\kappa_{\max}\eta$ remains higher than 1.5. Table I summarizes the relevant numerical parameters used in each of the simulations. From a physical point of view, the Reynolds number Re_0 and nondimensional distance z_f^* between the surface and the forcing region given in the table are built with the values of the turbulent kinetic energy k_0 and dissipation rate ϵ_0 at the surface. (From now on, the star superscript will denote a quantity normalized by these values.) With the choice of numerical parameters retained, the Reynolds-number range covered by our simulations goes from 76 to 302.

IV. ANALYSIS OF THE SIMULATION RESULTS

The flow obtained in the case Re=76 has been analyzed in details in Ref. 15 which gives the Reynolds stresses and length-scale profiles as well as the Reynolds-stress budgets across the flow. Here, we shall focus on the evolution of the quantities that help to define the spatial structure of the inhomogeneous layer, i.e., the Reynolds stresses and the vorticity variances.

A. Anisotropy of the Reynolds stresses and the blockage layer

Due to the symmetries of the problem, the Reynolds-stress tensor is diagonal and $\overline{u^2}=\overline{v^2}$ everywhere in the flow field. The profiles of the horizontal ($\overline{u^2}$) and vertical ($\overline{w^2}$) components of the Reynolds-stress tensor along the inhomogeneous direction z are plotted in Fig. 2 for the five data sets defined in Sec. III. All of them exhibit the typical behavior usually observed in free-surface turbulence. On top of the layer, both Reynolds stresses decrease at comparable rates as the surface is approached. Then, closer to the surface, the need to match the kinematic boundary condition leads to significantly different evolutions: the rate at which $\overline{w^2}$ decreases is enhanced, while it is the opposite for $\overline{u^2}$. In the latter case, the effect is so pronounced that $\overline{u^2}$ goes through a local minimum before increasing and finally reaching a local maximum at the surface. Such a maximum is also observed in the turbulent kinetic energy profiles (not shown here) and has been attributed to a reduction of the dissipation rate at the surface.[10,11,15]

The blockage layer is defined as this region across which the decrease of $\overline{w^2}$ is enhanced while that of $\overline{u^2}$ is reduced. Its

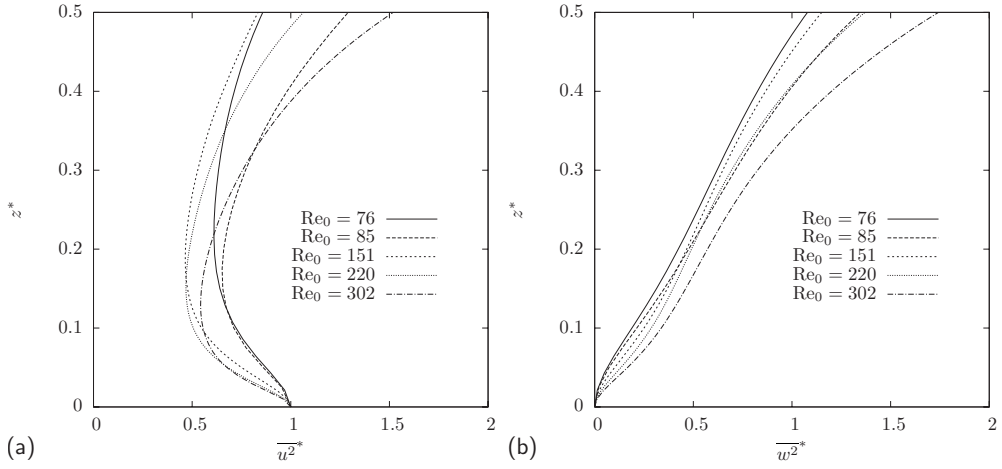

FIG. 2. Profiles of the Reynolds stresses above the surface. (a) $\overline{u^2}$ and (b) $\overline{w^2}$ [all quantities normalized by the turbulent scales at the surface (k_0,ϵ_0)].

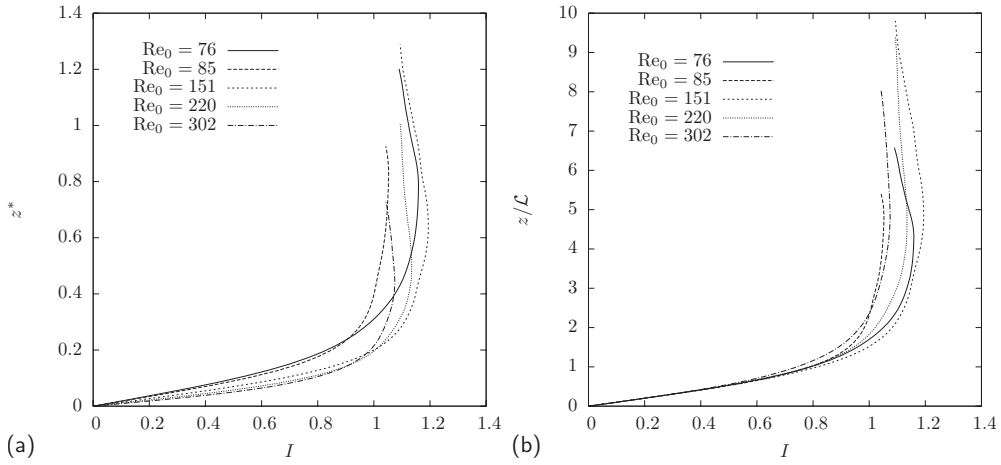

FIG. 3. Profiles of the isotropy parameter outside the turbulent-production region. (a) z is normalized by the turbulent scales at the surface $(k_0^{3/2}/\epsilon_0)$ and (b) z is normalized by the slope of the profile at the surface.

thickness δ_b can, in principle, be determined by considering the evolution of the isotropy parameter $I=w'/u'$: As mentioned in Sec. II, it should reach an equilibrium value in the self-diffusion region, it follows that the thickness of the blockage layer δ_b can be defined as the value of z below which I starts to decrease before going to zero at the surface. Examination of the isotropy-parameter profiles in Fig. 3 shows that they reach maxima scattered in a range of 1.05–1.2 which is typical of diffusing turbulence. However, the rather large scatter obtained indicates that for some of the data sets (at the lower end of the range), the distance between the production region and the surface is probably not sufficient for the flow to reach the self-similar state of purely diffusing turbulence so that the location of the maximum does not provide a precise measure of the blockage-layer thickness. On the other hand, the slopes of the profiles appear as slowly varying within a significant part of the blockage layer adjacent to the surface, which suggests that the gradient of the isotropy parameter at $z=0$ should behave as $1/\delta_b$. The length scale $\mathcal{L}=(dI/dz)_{z=0}^{-1}$ will therefore be introduced as a measure of δ_b that should not be too sensitive to the precise nature of the distant turbulence. The value of the isotropy parameter is plotted in Fig. 3(b) against $z/\mathcal{L}$. The plot shows that the effect of the kinematic boundary condition on the isotropy is felt at comparable distances (about $4.5-5\mathcal{L}$ from the surface) for all five data sets, thus supporting the idea according to which δ_b actually scales with $\mathcal{L}$. Values of $\mathcal{L}$ normalized by the turbulent scales at the surface are given for the five data sets in Table II.

TABLE II. Values of the blockage and slip-layer thicknesses obtained for the different data sets, the results are normalized by the turbulent scales at the surface k_0 and ϵ_0. The thickness δ_b can be estimated as $4.5-5\mathcal{L}$.

Re_0	76	85	151	220	302
$\mathcal{L}^*$	0.183	0.171	0.131	0.107	0.091
δ_s^*	0.0736	0.0736	0.0426	0.0346	0.0300

B. The normal velocity fluctuation and the Kolmogorov layer

The idea of a Kolmogorov layer was introduced by Brumley and Jirka.[14] The reasoning is that close to the surface and within a distance equal to the size of the smallest eddies (the Kolmogorov length scale), the flow can be assimilated to a pure stagnation flow due to the suppression of the horizontal vorticity component. Accordingly, the normal velocity fluctuation should follow its asymptotic linear behavior all across this region. Figure 4 shows the profiles of the normal rms fluctuation w' normalized by the Kolmogorov scales taken at the surface. One can check that the different curves closely follow the linear behavior for approximately one Kolmogorov length so that a scaling in the form

$$\delta_K^* = \frac{\delta_K}{k_0^{3/2}/\epsilon_0} \approx \frac{\nu^{3/4}\epsilon_0^{-1/4}}{k_0^{3/2}/\epsilon_0} = \mathrm{Re}_0^{-3/4} \tag{7}$$

can be retained for the thickness of the Kolmogorov layer. More interestingly, it appears that the slopes of the different profiles collapse at the surface: We find that

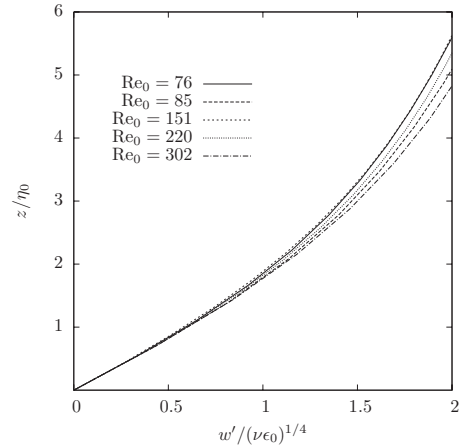

FIG. 4. Profiles of the rms normal velocity fluctuation scaled by the Kolmogorov scales at the surface (ν, ϵ_0).

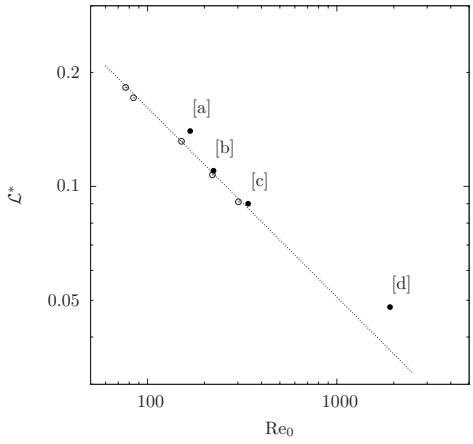

FIG. 5. Reynolds-number dependence of the outer layer thickness: $\mathcal{L}^*$ is plotted against the value of the turbulent Reynolds number at the surface. Open symbols, present data; dashed line, Eq. (9) with $A=0.62$; filled symbols, literature data with [a], Ref. 4, [b] Ref. 6, [c] Ref. 11, and [d] Ref. 13.

$$\frac{w'}{\nu^{1/4}\epsilon_0^{1/4}} = A \times \frac{z}{\nu^{3/4}\epsilon_0^{-1/4}} \tag{8}$$

within the Kolmogorov layer, where $A=0.62$ (with a scatter of only 1% within the Reynolds-number range involved here).

C. Outer (blockage-layer) scaling

We shall see now that the universality observed in the Kolmogorov layer for the profile of the normal velocity fluctuation directly leads to the outer (blockage-layer) scaling. From the definition of $\mathcal{L}$, it is easy to show that

$$\mathcal{L} = \left[\frac{d}{dz}\left(\frac{w'}{u'}\right)\right]_{z=0}^{-1} = \sqrt{k_0}\left.\frac{dw'}{dz}\right|_{z=0}^{-1}.$$

Equation (8) can then be used to express the rms-fluctuation derivative as

$$\left.\frac{dw'}{dz}\right|_{z=0} = A\epsilon_0^{1/2}\nu^{-1/2},$$

which leads to

$$\delta_b^* \propto \mathcal{L}^* = \frac{1}{A}\mathrm{Re}_0^{-1/2}. \tag{9}$$

The value obtained here for $\mathcal{L}^*$ as a function of the turbulent Reynolds number at the surface is plotted in Fig. 5 together with relation (9) and other data obtained from literature. The agreement between our data and the theoretical estimate is indeed very good since it follows directly from the very small scatter obtained here in the value of A. The other data used in the figure come from different flow configurations: An initially isotropic turbulence[11] or a time-evolving wake[6] in the presence of a free-surface, and open-channel flows.[4,13] Despite these differences in the structure of the distant turbulence, the corresponding data fall fairly close to the proposed Reynolds-number scaling. The largest discrepancy is observed with the LES data of Calmet and Magnaudet[13] for a high-Reynolds-number channel flow; even in this case, the value of $\mathcal{L}^*$ is not really at odds with the proposed scaling [it is about 0.058 in this flow when Eq. (9) gives 0.037].

D. Anisotropy of the vorticity components and the slip layer

A direct consequence of the dynamic, no-shear boundary condition at the surface is that the horizontal components of the vorticity vector vanish at the surface. The "inner" slip layer is defined as the region across which the fluctuating vorticity responds to this specific boundary condition. The profiles of the normal ($\overline{\omega_z^2}=\overline{\omega_z'^2}$) and tangential ($\overline{\omega_x^2}=\overline{\omega_x'^2}$) vorticity variances obtained in the five simulations can be seen in Fig. 6. The evolution of $\overline{\omega_x^2}$ clearly reveals the composite structure of the interaction layer with different behaviors in three distinct regions: On top of the layer, the behavior is typical of diffusing turbulence with $\overline{\omega_x^2}$ decreasing with the distance to the turbulence-production region. Entering the blockage layer, the decrease is interrupted; for the three highest values of the Reynolds number, $\overline{\omega_x^2}$ even experiences a slight increase before reaching a local maximum. Closer to the surface—in the slip layer—the variances return to zero as a result of the dynamic boundary condition at the surface. The evolution of the normal-vorticity variance in Fig. 6(b) mirrors that of $\overline{\omega_x^2}$: the rate at which $\overline{\omega_z^2}$ decreases is aug-

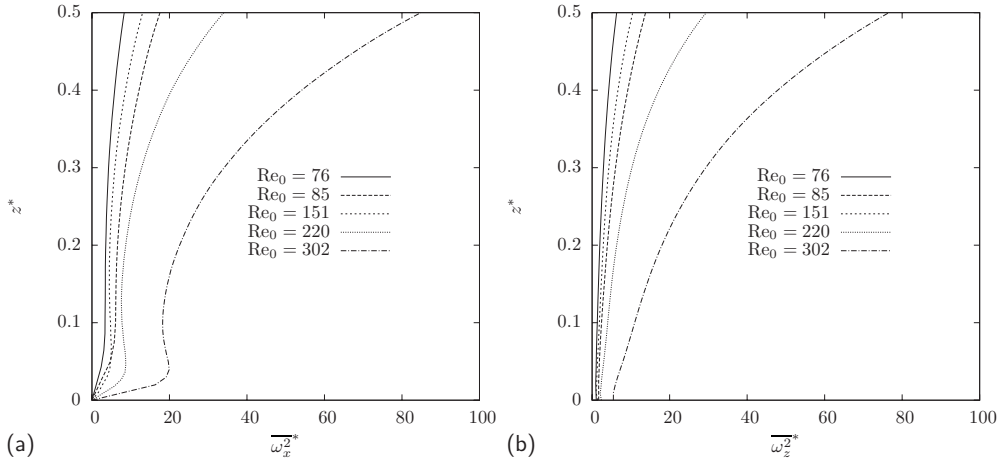

FIG. 6. Profiles of the vorticity variances above the surface. (a) $\overline{\omega_x^2}$ and (b) $\overline{\omega_z^2}$ [all quantities normalized by the turbulent scales at the surface (k_0, ϵ_0)].

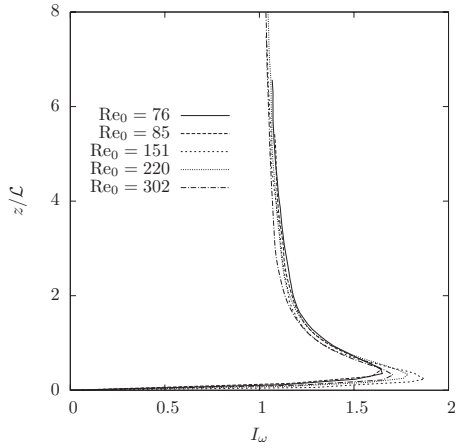

FIG. 7. Profiles of the *vorticity* isotropy parameter I_ω outside the turbulent-production region. z is normalized by the outer length scale $\mathcal{L}$.

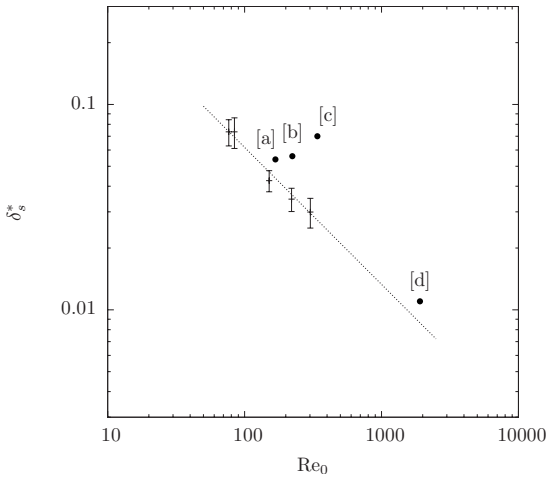

FIG. 8. Reynolds-number dependence of the slip-layer thickness. Error bars, present data; dashed line, Eq. (11); solid dots, literature data with [a] Ref. 4, [b] Ref. 6, [c] Ref. 11, and [d] Ref. 13.

mented in the top of the blockage layer, and diminished in the slip layer so as to reach a nonzero value at the surface.

Introducing an isotropy parameter for the fluctuating vorticity as $I_\omega = \omega_x'/\omega_z'$, the problem of a precise definition of the slip layer can be analyzed in a way very similar to that of the blockage layer. Figure 7 shows the evolution of this parameter for the five data sets, the vertical coordinate is normalized by $\mathcal{L}$. Starting from the outer edge of the blockage layer where it is close to unity, the value of the isotropy parameter can be seen to increase steadily across the blockage layer before reaching a maximum and then going to zero at the surface. Strikingly, all five profiles collapse within a small scatter in the region where I_ω increases with decreasing $z/\mathcal{L}$. There is little doubt that this is a blockage-layer effect, the increase in I_ω is obviously linked to the previously observed decrease in I in the same region, probably as a result of vortex stretching: Enstrophy budgets given by Shen *et al.*[6] indicate that the vortex-stretching term is an important contributor to the budget there, accordingly higher velocity fluctuations in the tangential direction should produce higher vorticity fluctuations in the same direction. Such collapse when the profiles are plotted against $z/\mathcal{L}$ supports our interpretation of $\mathcal{L}$ as a measure of the blocking effect. The picture changes in the slip layer, where the different profiles can be seen to peel off from the continuously increasing curve observed in the blockage layer (the profile would go to infinity at $z=0$ with a *no-slip* boundary condition) before going to zero. Strictly speaking, the thickness of the slip layer can be defined as the distance from the surface at which this peel-off occurs. Unfortunately, such a definition does not provide a practically efficient way to measure this quantity. It would be tempting to follow the same idea as that used to estimate the thickness of the blockage layer and base our measure of δ_s on the slope of the I_ω profile at the surface. However, this quantity is very sensitive to statistical-convergence and accuracy issues, and we have found it more convenient to define δ_s as the location in z at which the maximum of I_ω is reached. The corresponding results normalized by the turbulent scales at the surface are given in Table II.

E. Inner (slip-layer) scaling

Using the values obtained above for the thickness of the slip layer, we shall now look for a complete scaling of the near-surface flow in the form

$$\delta_b^* \propto \mathrm{Re}_0^{-1/2}, \quad \delta_s^* \propto \mathrm{Re}_0^{-\alpha}, \quad \text{and} \quad \delta_K^* \propto \mathrm{Re}_0^{-3/4}. \tag{10}$$

It is easy to show that consistency with the Hunt–Graham scaling [Eq. (3)] requires that $\alpha = 2/3$. Taking this value for the exponent, a least-square approximation to our data gives

$$\delta_s^* = 1.33\ \mathrm{Re}_0^{-2/3}. \tag{11}$$

This power law, together with our data and other literature data, is plotted in Fig. 8. The former are given within uncertainty bounds that correspond to the spatial resolution of the simulation. For the two channel-flow simulations taken from literature[4,13] and referenced as [a] and [d] on the graph, the $-2/3$ power law holds with a slightly higher constant: 1.67 instead of 1.33. The remaining literature data, denoted as [b] and [c], come from time-evolving flows[11,6] and are farther from Eq. (11). When extracting these data, we found that the maximum of I_ω was rather smooth so that our definition of δ_s is probably less reliable in this case. On the whole, we conclude that the location of the maximum is an adequate measure of the thickness of the slip layer (it confirms the $\mathrm{Re}_0^{-2/3}$ scaling) although it does not seem to yield a universal law, independent of the characteristics of the distant turbulence.

V. CONCLUSION

The DNSs performed in this work have allowed us to propose new scalings for the shearless turbulent boundary layer close to a free-slip surface. Accordingly, the thicknesses of the different sublayers can be explicitly related to the surface values of the turbulent kinetic energy and dissipation rate, and the corresponding Reynolds number. This is an important difference with previously proposed scalings for which reference quantities were taken at the edge of the blockage region or involved global quantities. The main ad-

vantage is that our scalings can be used in various types of free-surface flows whatever the distant turbulence-generation mechanism is.

In addition, it has been shown that the specific length-scale $\mathcal{L}$, built with the local (surface) characteristics of the anisotropy-parameter profile, measures the extent of the blockage effect into the flow (not proportional to the turbulent length scale at the surface $k_0^{3/2}/\epsilon_0$.) It is important to recall that its Reynolds-number dependency is a direct and exact consequence of the presence of the Kolmogorov layer. Our data bring convincing evidence of the presence of such a layer, the value of the normal-fluctuation gradient there being remarkably stable throughout the whole Reynolds-number range covered.

From a turbulence-modeling point of view, interesting outcomes are worthy of mention: At the first-order closure level, the surface references are available and the extent of the blockage effect can be measured through the relation $\mathcal{L} \propto k_0^{3/2}/\epsilon_0 \times \mathrm{Re}_0^{-1/2}$. At the second-order closure level, the isotropy parameter I is directly available and easy to relate to Lumley's flatness parameter $\mathcal{A}$ which is of more general use. [$\mathcal{A}=1-9(\mathrm{II}-\mathrm{III})/8$, where II and III are the second and third invariants of the anisotropy tensor $b_{ij}=\overline{u_i u_j}/k-2\delta_{ij}/3$.] In our flow (with $b_{11}=b_{22}$ and $b_{ij}=0$ if $i \neq j$), it is easy to show that

$$\mathcal{L} = (3/2)^{3/2}(d\sqrt{\mathcal{A}}/dz)_{z=0}^{-1}.$$

Transposition of this finding to the case of a solid wall is an important question that cannot be fully answered at this stage. However recent simulations by Bodart[24] seemed to indicate that all other things being equal, changing the free-surface boundary condition into a solid-wall boundary condition in the calculation of the same flow configuration, leaves the isotropy-parameter profile essentially unaltered, thus indicating that $\mathcal{L}$ could measure the extent of the blockage effect in both cases.

[1] S. Kumar, R. Gupta, and S. Banerjee, "An experimental investigation of the characteristics of free-surface in channel flow," Phys. Fluids **10**, 437 (1998).
[2] S. Komori, H. Ueda, F. Ogino, and T. Mizushina, "Turbulence structure in stably stratified open-channel flow," J. Fluid Mech. **130**, 13 (1983).
[3] K. Lam and S. Banerjee, "Investigation of turbulent flow bounded by a wall and a free surface," in *Fundamentals of Gas-Liquid Flows*, edited by E. Michaelides and M. P. Sharma (ASME, New York, 1988), p. 29.
[4] R. A. Handler, T. F. Swean, Jr., R. I. Leighton, and J. D. Swearingen, "Length scales and the energy balance for turbulence near a free surface," AIAA J. **31**, 1998 (1993).
[5] R. I. Leighton, T. F. Swean, R. Handler, and J. D. Swearingen, "Interaction of vorticity with a free surface in turbulent open channel flow," AIAA Paper No. 91-0236, 1991.
[6] L. Shen, X. Zhang, D. K. P. Yue, and G. S. Triantafyllou, "The surface layer for free-surface turbulent flows," J. Fluid Mech. **386**, 167 (1999).
[7] L. Shen, G. S. Triantafyllou, and D. K. P. Yue, "Turbulent diffusion near a free surface," J. Fluid Mech. **407**, 145 (2000).
[8] C. Zhang, L. Shen, and D. K. P. Yue, "The mechanism of vortex reconnection at a free surface," J. Fluid Mech. **384**, 207 (1999).
[9] B. H. Brumley and G. H. Jirka, "Near-surface turbulence in a grid-stirred tank," J. Fluid Mech. **183**, 235 (1987).
[10] B. Perot and P. Moin, "Shear-free turbulent boundary layers. Part 1. Physical insight into near-wall turbulence," J. Fluid Mech. **295**, 199 (1995).
[11] D. T. Walker, R. I. Leighton, and L. O. Garza-Rios, "Shear-free turbulence near a flat free surface," J. Fluid Mech. **320**, 19 (1996).
[12] J. C. R. Hunt and J. M. R. Graham, "Free-stream turbulence near plane boundaries," J. Fluid Mech. **84**, 209 (1978).
[13] I. Calmet and J. Magnaudet, "Statistical structure of high-Reynolds-number turbulence close to the free surface on an open-channel flow," J. Fluid Mech. **474**, 355 (2003).
[14] B. H. Brumley and G. H. Jirka, "Air-water transfer of slightly soluble gases: Turbulence, interfacial processes and conceptual models," PCH, PhysicoChem. Hydrodyn. **10**, 295 (1988).
[15] G. Campagne, J.-B. Cazalbou, L. Joly, and P. Chassaing, in *ECCOMAS CDF 2006*, edited by P. Wesseling, E. Oñate, and J. Périaux (TU Delft, The Netherlands, 2006).
[16] R. R. Long, "Theory of turbulence in a homogeneous fluid induced by an oscillating grid," Phys. Fluids **21**, 1887 (1978).
[17] S. M. Thompson and J. S. Turner, "Mixing across an interface due to turbulence generated by an oscillating grid," J. Fluid Mech. **67**, 349 (1975).
[18] E. J. Hopfinger and J.-A. Toly, "Spatially decaying turbulence and its relation to the mixing across density interfaces," J. Fluid Mech. **78**, 155 (1976).
[19] S. C. Dickinson and R. R. Long, "Laboratory study of the growth of a turbulent layer of fluid," Phys. Fluids **21**, 1698 (1978).
[20] E. Lamballais, "Simulations numériques de la turbulence dans un canal plan tournant," Ph.D. thesis, Institut National Polytechnique de Grenoble, 1996.
[21] S. A. Orszag, "Numerical methods for the simulation of turbulence," Phys. Fluids **12**, II-250 (1969).
[22] S. A. Orszag, "On the elimination of aliasing in finite difference schemes by filtering high wave number components," J. Atmos. Sci. **28**, 1074 (1971).
[23] K. Alvelius, "Random forcing of three-dimensional homogeneous turbulence," Phys. Fluids **11**, 1880 (1999).
[24] J. Bodart, Private communication, 2008.